ISSN 1063-7761, Journal of Experimental and Theoretical Physics, 2012, Vol. 115, No. 5, pp. 815–828. © Pleiades Publishing, Inc., 2012.
Original Russian Text © A.A. Demidov, I.A. Gudim, E.V. Eremin, 2012, published in Zhurnal Eksperimental'noi i Teoreticheskoi Fiziki, 2012, Vol. 142, No. 5, pp. 928–942.

ORDER, DISORDER, AND PHASE TRANSITION IN CONDENSED SYSTEM

Magnetic Properties of $Sm_{0.7}Ho_{0.3}Fe_3(BO_3)_4$

A. A. Demidov[a],*, I. A. Gudim[b], and E. V. Eremin[b]

[a] *Bryansk State Technical University, Bryansk, 241035 Russia*

* *e-mail: demandr@yandex.ru*

[b] *Kirensky Institute of Physics, Siberian Branch, Russian Academy of Sciences, Krasnoyarsk, 660038 Russia*

Received March 14, 2012

Abstract—The magnetic properties of a ferroborate single crystal of substituted composition $Sm_{0.7}H_{0.3}Fe_3(BO_3)_4$ with competing Sm–Fe and Ho–Fe exchange interactions are studied. The measured properties and effects are interpreted in terms of a general theoretical approach based on the molecular field approximation and calculations using the crystal field model for a rare-earth ion. The experimental temperature dependences of the initial magnetic susceptibility in the temperature range 2–300 K, the anomalies in the magnetization curves for $\mathbf{B} \parallel \mathbf{c}$ and $\mathbf{B} \perp \mathbf{c}$ in fields lower than 1.2 T, and the field and temperature dependences of magnetization in fields lower than 9 T are described. The crystal field parameters and the parameters of the R–Fe and Fe–Fe exchange interactions are determined during the interpretation of the experimental data.

DOI: 10.1134/S1063776112100020

INTRODUCTION

Trigonal rare-earth ferroborates $RFe_3(BO_3)_4$ (R = Y, La–Lu) are of particular interest for the physics of magnetic phenomena as *f–d* compounds with a specific interaction of their rare-earth and iron subsystems. Modern intense interest in the ferroborates is caused by the multiferroelectrical properties detected in them [1–3]. Since the discovery of new ferroborates of substituted compositions $R_{1-x}R'_xFe_3(BO_3)_4$, new possibilities for composition variations appeared and resulted in a variety of physical properties [4–9].

The iron subsystem in ferroborates becomes ordered at Néel temperatures $T_N \sim 30$–40 K. Their rare-earth subsystem is magnetized by an *f–d* interaction and makes a significant contribution to magnetic anisotropy and the orientation of magnetic moments. Ferroborates can be easy-axis (magnetic moments of R = Pr, Tb, Dy, Fe are oriented along the *c* axis of a crystal) or easy-plane (magnetic moments of R = Y, Nd, Sm, Eu, Er, Fe lie in the *ab* plane of a crystal) compounds or can pass spontaneously from the easy-axis to the easy-plane state, as in $GdFe_3(BO_3)_4$ and $HoFe_3(BO_3)_4$ (see, e.g., review [3]).

The belonging of the ferroborates of substituted composition $R_{1-x}R'_xFe_3(BO_3)_4$ to the class of multiferroics is being established [4, 6–8], and the effects caused by the competition of contributions, e.g., spontaneous reorientation transitions between the easy-axis and easy-plane states, can appear if competing R–Fe and R'–Fe exchange interactions are present in them [4–8].

The available spectroscopic [10], magnetic, magnetoelectric, and magnetoelastic [3, 11–13] information indicates that the magnetic moments of iron in $SmFe_3(BO_3)_4$ are antiferromagnetically ordered at $T_N \approx 32$–33 K and lie in the *ab* basal plane. Moreover, the magnetic moments of samarium magnetized by the exchange field of iron also lie in the basal plane. The magnetic moments of iron in $HoFe_3(BO_3)_4$ are antiferromagnetically ordered at $T_N \approx 38$ K and lie in the basal plane when the temperature decreases to $T_{SR} \approx 4.7$ K, as in the case of the magnetic moments of Ho^{3+} ions. A spontaneous spin-reorientation transition takes place at $T_{SR} \approx 4.7$ K; as a result, the magnetic moments of the Fe and Ho subsystems become oriented along the trigonal *c* axis [14–16]. Thus, spontaneous and magnetic field–induced spin-reorientation transitions from axis *c* to plane *ab*, which are similar to those detected recently in $Nd_{1-x}Dy_xFe_3(BO_3)_4$ (x = 0.1, 0.15, 0.25) [4, 17, 18], can result from the competition of the contributions of Sm^{3+} and Ho^{3+} ions to the magnetic anisotropy of substituted ferroborate $Sm_{1-x}Ho_xFe_3(BO_3)_4$.

Deep interest in the $SmFe_3(BO_3)_4$ ferroborate is also caused by the fact that it exhibits a giant magnetodielectric effect [12]. A giant (more than threefold) decrease in the permittivity takes place in a magnetic field of about 5 kOe applied in the basal plane of a crystal. The spontaneous and magnetic field–induced ($\mathbf{B} \parallel \mathbf{a}$) spin-reorientation transitions in $HoFe_3(BO_3)_4$ and the spin-flop transition at $\mathbf{B} \parallel \mathbf{c}$ in it were theoretically studied in [19]. The spontaneous spin-reorientation transition was shown to be a magnetic analog of the Jahn–Teller effect, and the crystal field parameters for the Ho^{3+} ion in $HoFe_3(BO_3)_4$ and the parameters of the exchange Ho–Fe and Fe–Fe interactions were determined.

The purpose of this work is to study the low-temperature magnetic properties of $Sm_{0.7}Ho_{0.3}Fe_3(BO_3)_4$ experimentally and theoretically, to compare the obtained experimental data with the results of calculations performed in terms of a general theoretical approach, and to determine the compound parameters.

EXPERIMENTAL

Single crystals were grown from solution melts based on bismuth trimolybdate 80 wt % $\{Bi_2Mo_3O_{12} + 3B_2O_3 + 0.6[(1 - x)Sm_2O_{3+x}Ho_2O_3]\}$ + 20 wt % $Sm_{1-x}Ho_xFe_3(BO_3)_4$ in accordance with the technique described in detail in [5]. The crystals were simultaneously grown in a 150-g solution–melt on four seeds with a volume of approximately 1 mm^3 under identical hydrodynamic conditions. The crystal holder was reversibly rotated at a speed of 30 rpm and a period of 1 min. The supercooling corresponded to an increase in the crystal height less than 1 mm/day. After the end of growth, the crystal holder was lifted above the solution–melt, and the crystals were cooled to room temperature in a switched-off furnace. The grown crystals with a height of 6–10 mm had a small triangular {0001} pinacoid face perpendicular to the C_3 axis. Samples of the required orientations were prepared according to the crystal morphology. They had a good optical quality and had no visible defects. The samarium and holmium contents in a crystal were determined by X-ray spectral fluorescent analysis. Magnetic measurements were performed on a Physical Properties Measurement System (Quantum Design) device in the temperature range 2–300 K and magnetic fields up to 9 T.

COMPUTATIONAL TECHNIQUE

The magnetic properties of $Sm_{1-x}Ho_xFe_3(BO_3)_4$ ferroborates are determined by both magnetic subsystems, i.e., the rare-earth (samarium and holmium) subsystem and the iron subsystem, which interact with each other. The interaction within the R subsystem can be neglected, since none of the ferroborates and isostructural aluminoborates exhibits self-ordering in the R subsystem. The iron subsystem can be considered as a set of two antiferromagnetic sublattices. The R subsystem magnetized due to the *f–d* interaction can also be represented in the form of two sublattices.

In our calculations, we used the theoretical approach that was successfully employed for pure ferroborates $RFe_3(BO_3)_4$ with R = Tb [20], Nd [21], Dy [22], Pr [23], Ho [19], and Er [24] and for ferroborates with substituted compositions $Nd_{1-x}Dy_xFe_3(BO_3)_4$ [17, 18] and $Tb_{0.25}Er_{0.75}Fe_3(BO_3)_4$ [24]. This theoretical approach is based on the crystal field model for the R subsystem and the molecular field approximation.

Based on the magnetic structure and the hierarchy of the interactions in $Sm_{1-x}Ho_xFe_3(BO_3)_4$, we can write the effective Hamiltonians of an R/Fe ion of the ith ($i = 1, 2$) sublattice in magnetic field $\mathbf{B}$ in the form

$$\mathcal{H}_i(\mathrm{R}) = \mathcal{H}_i^{CF} + g_J^{\mathrm{R}}\mu_{\mathrm{B}}\mathbf{J}_i^{\mathrm{R}}[\mathbf{B} + \lambda_{fd}^{\mathrm{R}}\mathbf{M}_i^{\mathrm{Fe}}], \quad (1)$$

$$\mathcal{H}_i(\mathrm{Fe}) = g_S\mu_{\mathrm{B}}\mathbf{S}_i[\mathbf{B} + \lambda\mathbf{M}_i^{\mathrm{Fe}} + (1-x)\lambda_{fd}^{\mathrm{Sm}}\mathbf{m}_i^{\mathrm{Sm}} + x\lambda_{fd}^{\mathrm{Ho}}\mathbf{m}_i^{\mathrm{Ho}}], \quad j = 1, 2, \quad j \neq i. \quad (2)$$

Here, $\mathcal{H}^{CF}$ is the crystal field Hamiltonian, g_J^{R} is the Lande factor, $\mathbf{J}_i^{\mathrm{R}}$ is the angular momentum operator for the R ion, $g_S = 2$ is the g factor, $\mathbf{S}_i$ is the spin moment operator for the Fe ion, and $\lambda_{fd}^{\mathrm{R}} < 0$ and $\lambda < 0$ are the molecular constants of the R–Fe and Fe–Fe antiferromagnetic interactions.

The magnetic moments of the ith iron ($\mathbf{M}_i^{\mathrm{Fe}}$) and rare-earth ($\mathbf{m}_i^{\mathrm{R}}$) sublattices per formula unit are determined by the following relationships:

$$\mathbf{M}_i^{\mathrm{Fe}} = -3g_S\mu_{\mathrm{B}}\langle\mathbf{S}_i\rangle, \quad \mathbf{m}_i^{\mathrm{R}} = -g_J^{\mathrm{R}}\mu_{\mathrm{B}}\langle\mathbf{J}_i^{\mathrm{R}}\rangle. \quad (3)$$

The right-hand side of the equation for $\mathbf{M}_i^{\mathrm{Fe}}$ is the Brillouin function that forms in the case of an equidistant spectrum of the Fe^{3+} S ion for thermal mean $\langle S_i\rangle$. The Fe^{3+} ion in $RFe_3(BO_3)_4$ is in a high-spin state [25], which gives the maximum magnetic moment of the ion ($5\mu_{\mathrm{B}}$).

The local symmetry of the environment of the Ho^{3+} ion in $HoFe_3(BO_3)_4$ at high temperatures is described by point group D_3. A structural transition takes place in $HoFe_3(BO_3)_4$ near $T = 420$ K [25]; however, the related decrease in the symmetry is likely to affect the thermodynamic properties of $HoFe_3(BO_3)_4$ weakly, as in the case of the structural transition in $GdFe_3(BO_3)_4$ at $T = 156$ K [26]. $SmFe_3(BO_3)_4$ does not exhibit a structural transition with a decrease in the symmetry. There is no information on the existence of a possible structural transition in ferroborates $Sm_{1-x}Ho_xFe_3(BO_3)_4$. Then, for $Sm_{0.7}Ho_{0.3}Fe_3(BO_3)_4$ we may assume that, as the temperature decreases, the noted symmetry is retained or the appearing deviations from symmetry D_3 are too small to affect the thermodynamic properties. In the Wybourne setting for group D_3 (where axis c is a trigonal axis and a twofold axis coincides with axis a) [27], an expression for crystal field Hamiltonian $\mathcal{H}^{CF}$ in terms of irreducible tensor operators C_q^k has the form

$$\mathcal{H}^{CF} = B_0^2C_0^2 + B_0^4C_0^4 + B_3^4(C_{-3}^4 - C_3^4) + B_0^6C_0^6 + B_3^6(C_{-3}^6 - C_3^6) + B_6^6(C_{-6}^6 + C_6^6). \quad (4)$$

Crystal field parameters B_q^k for the Sm^{3+} and Ho^{3+} ions in $Sm_{1-x}Ho_xFe_3(BO_3)_4$ are unknown. Exact information concerning the splitting of the ground multiplet of the Sm^{3+} and Ho^{3+} ions in $Sm_{1-x}Ho_xFe_3(BO_3)_4$ is not available either. It is known from the spectroscopic studies [10] that the splitting of the ground doublet of the Sm^{3+} ion in $SmFe_3(BO_3)_4$ is $\Delta = 13.2$ cm^{-1} and that the lower part of the Sm^{3+} ion is characterized by energies of 0, 135, and 220 cm^{-1}. The crystal field parameters for the Ho^{3+} ion in $HoFe_3(BO_3)_4$, which were used to describe extensive experimental data on the magnetic properties, we found in [19]. Note that crystal field Hamiltonian (4) for the Sm^{3+} ion only has three terms (with B_0^2, B_0^4, and B_3^4), since the matrix elements are nonzero only at $k < 2J$, i.e., in the case of Sm ($J = 5/2$) $k < 5$ (see, e.g., [28]).

The computation of the values and orientations of the magnetic moments of the Fe and R subsystems in solving the self-consistent problems using Hamiltonians (1) and (2) at the minimum of the corresponding thermodynamic potential makes it possible to calculate the stability regions of various magnetic phases, the phase-transition fields, magnetization curves, the susceptibility, and so on. In terms of the standard thermodynamic perturbation theory described in monograph [21] for *f–d* compounds, the thermodynamic potential can be written as

$$\begin{aligned}\Phi(T, B) = \frac{1}{2}\sum_{i=1}^{2}\Big[&-(1-x)k_BT\ln Z_i(\mathrm{Sm})\\ &- xk_BT\ln Z_i(\mathrm{Ho}) + (1-x)\frac{1}{2}g_J^{\mathrm{Sm}}\mu_B\langle \mathbf{J}_i^{\mathrm{Sm}}\rangle\lambda_{fd}^{\mathrm{Sm}}\mathbf{M}_i^{\mathrm{Fe}}\\ &+ x\frac{1}{2}g_J^{\mathrm{Ho}}\mu_B\langle \mathbf{J}_i^{\mathrm{Ho}}\rangle\lambda_{fd}^{\mathrm{Ho}}\mathbf{M}_i^{\mathrm{Fe}} - 3k_BT\ln Z_i(\mathrm{Fe})\\ &+ \frac{1}{2}3g_S\mu_B\langle \mathbf{S}_i\rangle(\lambda\mathbf{M}_i^{\mathrm{Fe}} + (1-x)\lambda_{fd}^{\mathrm{Sm}}\mathbf{m}_i^{\mathrm{Sm}}\\ &+ x\lambda_{fd}^{\mathrm{Ho}}\mathbf{m}_i^{\mathrm{Ho}}) + \Phi_{\mathrm{an}}^i\Big],\end{aligned} \tag{5}$$

where Z_i(R/Fe) are the partition sums calculated with Hamiltonians (1) and (2) and Φ_{an}^i is the anisotropy energy for the *i*th sublattice of the Fe system, which is much lower than the exchange energy and, hence, can be written as an additive term. For a crystal of trigonal symmetry (see, e.g., [29]), this energy is

$$\begin{aligned}\Phi_{\mathrm{an}}^i &= K_2^{\mathrm{Fe}}\sin^2\vartheta_i + K_4^{\mathrm{Fe}}\sin^4\vartheta_i + K_6^{\mathrm{Fe}}\sin^6\vartheta_i\\ &+ K_{33}^{\mathrm{Fe}}\cos\vartheta_i\sin^3\vartheta_i\sin 3\varphi_i + K_{66}^{\mathrm{Fe}}\sin^6\vartheta_i\cos 6\varphi_i,\end{aligned} \tag{6}$$

where anisotropy constant $K_2^{\mathrm{Fe}} < 0$ stabilizes the easy-plane antiferromagnetic state; constants $K_4^{\mathrm{Fe}} > 0$ and $K_6^{\mathrm{Fe}} > 0$ stabilize the easy-axis state; $K_{33}^{\mathrm{Fe}} < 0$ and $K_{66}^{\mathrm{Fe}} < 0$ are the anisotropy constants in the *ab* basal plane; and ϑ_i and φ_i are the polar and azimuth angles of magnetic moment vector $\mathbf{M}_i^{\mathrm{Fe}}$ of iron, respectively.

Three types of domains can exist in a trigonal crystal with magnetic moments lying in the basal plane. The magnetization of $Sm_{1-x}Ho_xFe_3(BO_3)_4$ (per formula unit with allowance for possible existence of three types of domains, $n = 1, 2, 3$) is

$$\mathbf{M} = \frac{1}{3}\sum_{n=1}^{3}\frac{1}{2}\sum_{i=1}^{2}(\mathbf{M}_i^{\mathrm{Fe}} + (1-x)\mathbf{m}_i^{\mathrm{Sm}} + x\mathbf{m}_i^{\mathrm{Ho}}). \tag{7}$$

The rare-earth and iron subsystems contribute to the magnetic susceptibility of $Sm_{1-x}Ho_xFe_3(BO_3)_4$ as follows:

$$\chi_k = \chi_k^{\mathrm{Fe}} + (1-x)\chi_k^{\mathrm{Sm}} + x\chi_k^{\mathrm{Ho}}, \quad k = a, b, c. \tag{8}$$

In the ordered phase, the initial magnetic susceptibilities of the compound can be found from the linear segments of the magnetization curves calculated for the corresponding directions of an external magnetic field. In the paramagnetic region (where the interaction between the R and Fe subsystems can be neglected), the magnetic susceptibility of the R subsystem can be calculated using the well-known Van Vleck formula, the energy spectrum and wavefunctions for which are calculated using crystal field Hamiltonian (4). Susceptibility χ_p^{Fe} of the Fe subsystem can be described by the Curie–Weiss law with the corresponding paramagnetic Néel temperature Θ,

$$\begin{aligned}\chi_p^{\mathrm{Fe}} &= \frac{\mu_{\mathrm{eff}}^2}{3k_B(T-\Theta)},\\ \mu_{\mathrm{eff}}^2 &= 105\mu_B^2 \text{ for } S = \frac{5}{2}.\end{aligned} \tag{9}$$

RESULTS AND DISCUSSION

To determine the parameters of the crystal field (which forms the electronic structure of a rare-earth ion), we used the experimental data for the temperature dependences of the initial magnetic susceptibility of $Sm_{0.7}Ho_{0.3}Fe_3(BO_3)_4$ along the trigonal axis and in the basal plane $\chi_{c,\perp c}(T)$ in the paramagnetic range from $T_N \approx 35$ K to $T_N \approx 300$ K. As the initial values of crystal field parameters B_q^k, we took the parameters for ferroborate $HoFe_3(BO_3)_4$ studied earlier [19]. For each of the found sets of B_q^k parameters, we chose those that describe susceptibilities $\chi_c(T)$ and $\chi_{\perp c}(T)$ in

Table 1. Energies of the lower levels of the ground multiplet of the Sm^{3+} (six levels) and Ho^{3+} (nine levels) ions in $Sm_{0.7}Ho_{0.3}Fe_3(BO_3)_4$ that are split by the crystal field (parameter (10)) with allowance for the *f–d* interaction at $B = 0$ in the paramagnetic and ordered temperature ranges

R	T	$\Delta = E_i - E_1$, cm^{-1} ($i^{Sm} = 6$, $i^{Ho} = 9$)
Sm	$T > T_N$	0, 0, 145, 145, 153, 153
	$T = 2$ K	0, 10.6, 145, 151, 157.4, 165
Ho	$T > T_N$	0, 4.3, 4.3, 34.8, 37.8, 37.8, 134, 166, 166
	$T = 2$ K	0, 7.8, 13.7, 37.8, 42.8, 47.8, 139, 167, 176

the paramagnetic region best of all. The paramagnetic Néel temperature for the Fe subsystem was found to be approximately the same, $\Theta = -170$ K. To determine which of the found sets of B_q^k parameters can describe the entire set of the measured magnetic characteristics of $Sm_{0.7}Ho_{0.3}Fe_3(BO_3)_4$, we calculated the magnetization along the trigonal axis and in the basal plane ($M_{c,\perp c}(B)$) at $T = 2$ K to choose parameters λ_{fd}^R (antiferromagnetic Sm–Fe and Ho–Fe interactions) and λ_1 (intrachain antiferromagnetic Fe–Fe interaction).

Thus, following these criteria of describing the $\lambda_{c,\perp c}(T)$ and $M_{c,\perp c}(T)$ curves and a small difference from the parameters from [19], we chose the set among the crystal field parameters found at the initial stage that ensures the best description of the experimental data (B_q^k, in cm^{-1}),

$$B_0^2 = 612, \quad B_0^4 = -2270, \quad B_3^4 = -825, \quad B_0^6 = 200, \quad B_3^6 = -55, \quad B_6^6 = 490. \tag{10}$$

These parameters were determined in the calculations based on the ground multiplet; therefore, they can be treated only as effective parameters suitable for describing the thermodynamic properties of $Sm_{0.7}Ho_{0.3}Fe_3(BO_3)_4$.

The set of parameters (10) corresponds to the energies of the lower levels of the ground multiplet of the Sm^{3+} and Ho^{3+} ions in $Sm_{0.7}Ho_{0.3}Fe_3(BO_3)_4$ that are given in Table 1 for $B = 0$. These energies are given for $T > T_N$ and with allowance for the *f–d* interaction at $T = 2$ K. As follows from Table 1, taking into account the *f–d* interaction at $T < T_N$ removes the degeneracy of the lower levels of the Sm^{3+} and Ho^{3+} ions, and the low-temperature splitting of the ground doublet of the Sm^{3+} ion in $Sm_{0.7}Ho_{0.3}Fe_3(BO_3)_4$ ($\Delta = 10.6$ cm^{-1}) agrees with the splitting of the ground doublet of the Sm^{3+} ion in $SmFe_3(BO_3)_4$ ($\Delta = 13.2$ cm^{-1}) [10, 13]. Note that $\Delta = 13.2$ cm^{-1} in [10, 13] was presented for easy-plane $SmFe_3(BO_3)_4$ and that the comparison is correct when $Sm_{0.7}Ho_{0.3}Fe_3(BO_3)_4$ is also in the easy-plane state (the splittings at $T = 2$ K in Table 1 are given for a state that differs from the easy-plane state; see text below). In the easy-plane state of $Sm_{0.7}Ho_{0.3}Fe_3(BO_3)_4$, parameters (10) correspond to the low-temperature splitting of the ground doublet of the Sm^{3+} ion $\Delta = 12$ cm^{-1}, which is closer to $\Delta = 13.2$ cm^{-1} from [10, 13]. The energies of the lower levels of the ground multiplet of the Ho^{3+} ion in $Sm_{0.7}Ho_{0.3}Fe_3(BO_3)_4$ are also close to those found for the Ho^{3+} ion in $HoFe_3(BO_3)_4$ in [19].

The calculated magnetic characteristics presented below in the figures were calculated for the parameters given in Table 2, which also gives the parameters of $HoFe_3(BO_3)_4$ [19] and the well-known reported data for $SmFe_3(BO_3)_4$ [10–13] for comparison. Parameter λ_2 in Table 2 enters into the Brillouin function, is responsible for the magnetic moment of Fe (at given T and B), and determines the Néel temperature, since the three-dimensional order in the structure of a ferroborate cannot exist without the exchange interaction between Fe^{3+} ion chains. The value of parameter λ_2 was chosen from the condition of the best agreement between the calculated and experimental $M_{c,\perp c}(B)$ curves at all temperatures. In the calculations, we also use the uniaxial anisotropy constants of iron ($K_2^{Fe} = -3.75$ T μ_B, $K_4^{Fe} = 4.41$ T μ_B, $K_6^{Fe} = 0.57$ T μ_B at $T = 4.2$ K) and the anisotropy constants of iron in the basal plane ($K_{33}^{Fe} = -0.69$ T μ_B, $K_{66}^{Fe} = -1.35 \times 10^{-2}$ T μ_B) [21].

As follows from Table 2, the *f–d* exchange interaction field for the Sm subsystem in $Sm_{0.7}Ho_{0.3}Fe_3(BO_3)_4$ ($B_{fd}^{Sm} = 36$ T) and the corresponding constant $\lambda_{fd}^{Sm} = -2.4$ T/μ_B are higher than those in the ferroborates studied earlier (see [20, 23] and the tables in [17, 22, 24]). This difference is caused by the specific feature of the ground multiplet of the Sm^{3+} ions, namely, a low Lande factor ($g_J^{Sm} = 2/7$) and, hence, a weakening of Zeeman splitting ($g_J^{Sm}\mu_B \mathbf{J}_i^{Sm}\mathbf{B}$) and the effect of the *f–d* exchange field (see Hamiltonian (1)). Moreover, $B_{fd}^{Sm} = 36$ T also yields a splitting of $\Delta = 12$ cm^{-1} for the ground doublet of the Sm^{3+} ion in the easy-plane state of $Sm_{0.7}Ho_{0.3}Fe_3(BO_3)_4$, which agrees with the splitting of the ground doublet of the Sm^{3+} ion in easy-plane $Sm_{0.7}Ho_{0.3}Fe_3(BO_3)_4$ [10, 13].

Note that the critical field in which the sign of electric polarization and magnetostriction in $SmFe_3(BO_3)_4$ changes is 30 T [11] (the sign changes at the fields that are equal to the *f–d* exchange interaction field [2]) and that this field agrees with the *f–d* exchange interaction field found for the Sm subsystem in $Sm_{0.7}Ho_{0.3}Fe_3(BO_3)_4$ ($B_{fd}^{Sm} = 36$ T). In this case, the field of 30 T for $SmFe_3(BO_3)_4$ was obtained using the *f–d* exchange interaction field in $NdFe_3(BO_3)_4$, which

Table 2. Parameters of $Sm_{0.7}Ho_{0.3}Fe_3(BO_3)_4$, $HoFe_3(BO_3)_4$ [19], and $SmFe_3(BO_3)_4$ [10–13]

Compound	$SmFe_3(BO_3)_4$	$Sm_{0.7}Ho_{0.3}Fe_3(BO_3)_4$	$HoFe_3(BO_3)_4$
$B_{dd1} = \lambda_1 M_0$, T		59.5	84
λ_1, T/μ_B		−3.97	−5.6
$B_{dd2} = \lambda_2 M_0$, T		27	27
λ_2, T/μ_B		−1.8	−1.8
$B_{fd} = \lambda_{fd}^R M_0$, T	30 [11]	36 (Sm) 2.85 (Ho)	2.5
λ_{fd}^R, T/μ_B		−2.4 (Sm) −0.19 (Ho)	−0.16
$\Delta_{fd} = \mu_B g\lvert\lambda_{fd}\rvert M_0$, cm^{-1}	13.2 (EP) [10] 13.2 (EP) [13]	~10.6 (CEMA) Sm ~7.8 (CEMA) Ho	~7.7 (EA) ~3.4 (EP)
ϑ_1, deg ($B = 0$)	$\vartheta_1 \to 90°$	$T = 2$, $\vartheta_1 \approx 63°$ $T = 4.2$, $\vartheta_1 \approx 65.5°$ $T = 30$, $\vartheta_1 \approx 70°$	$T_{SR} \approx 4.7$ K $\vartheta_1 \to 0$ ($T < T_{SR}$) $\vartheta_1 \to 90°$ ($T > T_{SR}$)
T_N, K	32 ± 1 [10] 33 [12]	35	38 [14]
Θ, K		−170	−210

Note: B_{dd1} (intrachain Fe–Fe), B_{dd2} (interchain Fe–Fe), and B_{fd} are the low-temperature exchange fields corresponding to molecular constants λ_1, λ_2, and λ_{fd}^R, respectively. Δ_{fd} is the low-temperature splitting of the ground state of an R ion due to the f–d interaction in the following states: a cone of easy magnetization axes (CEMA), easy-axis (EA) state, and easy-plane (EP) state. ϑ_1 is the angle of deviation of $\mathbf{M}_1^{Fe}$ from axis c. Θ is the paramagnetic Néel temperature for the Fe subsystem. $M_0 = |M_i(T = 0, B = 0)| = 15\mu_B$ is the magnetic moment of iron per formula unit.

is 5 T (see Eq. (3) and the related conclusions in [11]). If we substitute the f–d exchange interaction field for $NdFe_3(BO_3)_4$ from [21] ($B_{fd}^{Nd} = 7.1$ T) into Eq. (3) from [11] (we use the theoretical approach from [21] in this work for $Sm_{0.7}Ho_{0.3}Fe_3(BO_3)_4$), the critical field of changing the sign of electric polarization and magnetostriction in $SmFe_3(BO_3)_4$ is 42.6 T, which also agrees with the field found for $Sm_{0.7}Ho_{0.3}Fe_3(BO_3)_4$ ($B_{fd}^{Sm} = 36$ T).

To calculate the magnetic characteristics of $Sm_{0.7}Ho_{0.3}Fe_3(BO_3)_4$ in a magnetic field applied along and perpendicular to trigonal axis c, we used the scheme of the orientations of the magnetic moments of iron ($\mathbf{M}_i^{Fe}$) and rare earth ($\mathbf{m}_i^R$) shown in Fig. 1. The calculations according to the schemes in Figs. 1a and 1d were performed for a field directed along the trigonal axis ($\mathbf{B} \parallel \mathbf{c}$). The schemes in Figs. 1b and 1e were used for the case of a magnetic field oriented in the basal plane ($\mathbf{B} \perp \mathbf{c}$), and the scheme in Fig. 1c is shown for the case of $B = 0$ (cone of easy magnetization axes). The directions of the resulting magnetic moments of the R subsystem ($\mathbf{m}_i = (1 - x)\mathbf{m}_i^{Sm} + x\mathbf{m}_i^{Ho}$) and their projections along the field direction ($\mathbf{m}_{iab}$, $\mathbf{m}_{ia}$, $\mathbf{m}_{ic}$) are shown. We also depict the projections of the magnetic moments of Fe onto the ab plane ($\mathbf{M}_{iab}^{Fe}$) in domains with antiferromagnetism axes making angles $\varphi_i = 0°$ (L_0) and 60° (L_{60}) with the a axis.

The low-temperature magnetic state of substituted ferroborate $Sm_{0.7}Ho_{0.3}Fe_3(BO_3)_4$ is unknown. It is known that, at $B > 1.5$ T, ferroborate $HoFe_3(BO_3)_4$ is in the flop phase and behaves like a single-domain compound and that the magnetic moments of the Fe and Ho subsystems lie in the ab basal plane [19]. Then, allowing for an easy-plane character of the magnetic subsystem of $SmFe_3(BO_3)_4$, we first consider the magnetic properties of $Sm_{0.7}Ho_{0.3}Fe_3(BO_3)_4$ in fields higher than 1.5 T (single-domain state) and assume that its magnetic subsystem at $B > 1.5$ T exhibits easy-plane properties (Fig. 1a for $\mathbf{B} \parallel \mathbf{c}$ and Fig. 1b for $\mathbf{B} \perp \mathbf{c}$). In this state, the magnetic moments of the Fe sublattices $\mathbf{M}_1^{Fe}$ and $\mathbf{M}_2^{Fe}$ bend toward the field direction, manifesting susceptibility in the perpendicular direction (which is temperature independent for a typical antiferromagnet, and the component of the mag-

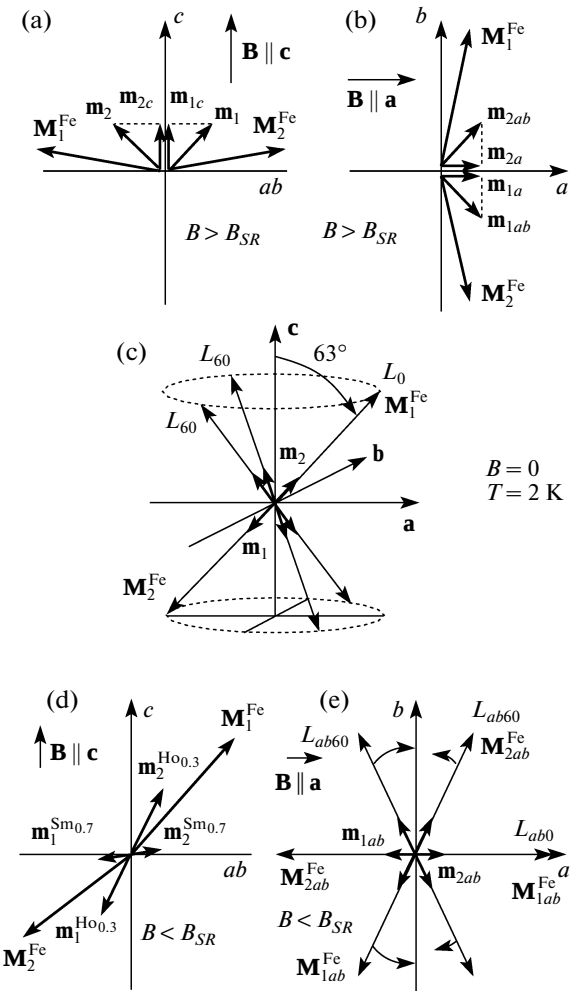

Fig. 1. Schematic diagrams for the orientations of the magnetic moments of iron ($\mathbf{M}_i^{Fe}$) and a rare-earth element ($\mathbf{m}_i^{R}$) used to calculate the magnetic properties of $Sm_{0.7}Ho_{0.3}Fe_3(BO_3)_4$ for various magnetic field directions. $\mathbf{m}_{ic}$, $\mathbf{m}_{ia}$, and $\mathbf{m}_{iab}$ are the projections of the magnetic moments of the *R* subsystem along the field direction. (a), (d) $\mathbf{B} \parallel \mathbf{c}$ (plane *ab* is perpendicular to the figure plane); (b), (e) $\mathbf{B} \parallel \mathbf{a}$ (axis *c* is perpendicular to the figure plane); (c) $B = 0$ (cone of easy magnetization axes).

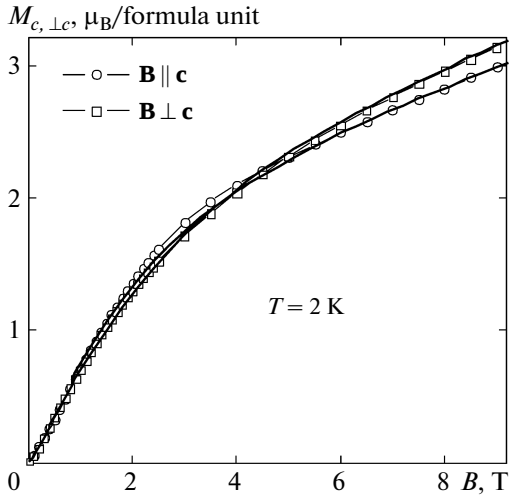

Fig. 2. Magnetization curves of $Sm_{0.7}Ho_{0.3}Fe_3(BO_3)_4$ for $\mathbf{B} \parallel \mathbf{c}$ and $\mathbf{B} \perp \mathbf{c}$ at $T = 2$ K: (symbols) experimental data and (lines) calculation.

netic moment of the *R* subsystem along the field direction increases.

As is seen from the experimental and calculated $M_{c,\perp c}(B)$ magnetization curves of $Sm_{0.7}Ho_{0.3}Fe_3(BO_3)_4$ at $T = 2$ K (Fig. 2), the $M_c(B)$ and $M_{c,\perp c}(B)$ curves increase monotonically with the field and demonstrate a low anisotropy along the $\mathbf{B} \parallel \mathbf{c}$ and $\mathbf{B} \perp \mathbf{c}$ directions. In $HoFe_3(BO_3)_4$, the $M_{c,\perp c}(B)$ magnetization curves in the field range 1–5 T also almost coincide [14, 16]. A low anisotropy during magnetization along $\mathbf{B} \parallel \mathbf{c}$ and $\mathbf{B} \perp \mathbf{c}$ was also detected in $SmFe_3(BO_3)_4$ at $B > 1$ T [30].

Figures 3 and 4 show the experimental and calculated magnetization curves for fields up to 9 T along the trigonal axis ($M_c(B)$, Fig. 3) and in the basal plane ($M_{\perp c}(B)$, Fig. 4) in the temperature range $T = 5$–40 K. As the temperature increases, the $M_{c,\perp c}(B)$ magnetization curves are seen to become less sharp and to change because of a decrease in the magnetic moments of the *R* and Fe subsystems. The characters of magnetization of $Sm_{0.7}Ho_{0.3}Fe_3(BO_3)_4$ in the basal plane and along the trigonal axis differ weakly, which indicates a weakly anisotropic contribution of the rare-earth subsystem induced by the crystal field of the samarium–holmium ferroborate. As follows from Figs. 2–4, the calculations on the assumption of the easy-plane state of $Sm_{0.7}Ho_{0.3}Fe_3(BO_3)_4$ at $B > 1.5$ T can correctly describe the behavior of the $M_{c,\perp c}(B)$ curves and their temperature dependences, which are similar to the experimental dependences.

The initial magnetic susceptibility of $Sm_{0.7}Ho_{0.3}Fe_3(BO_3)_4$ is contributed by both the iron subsystem ordered at $T < T_N$ and the rare-earth subsystem magnetized by the *f*–*d* interaction (predominant contribution from the Ho subsystem). The $\chi_{c,\perp c}(T)$ curves of $SmFe_3(BO_3)_4$ almost fully coincide with the magnetic susceptibility of $YFe_3(BO_3)_4$ [3], which points to a low magnetic contribution of the Sm subsystem to the magnetic characteristics. Figure 5 shows the experimental and calculated temperature dependences of the initial magnetic susceptibilities $\chi_{c,\perp c}(T)$ of $Sm_{0.7}Ho_{0.3}Fe_3(BO_3)_4$. The unique weakly anisotropic behavior (which differs from all ferroborates under study) of the experimental $\chi_{c,\perp c}(T)$ curves is clearly visible. The almost isotropic behavior of the $\chi_{c,\perp c}(T)$ curves detected in $Sm_{0.7}Ho_{0.3}Fe_3(BO_3)_4$ occurs over almost the entire temperature range except for the lowest temperatures at $T < 10$ K.

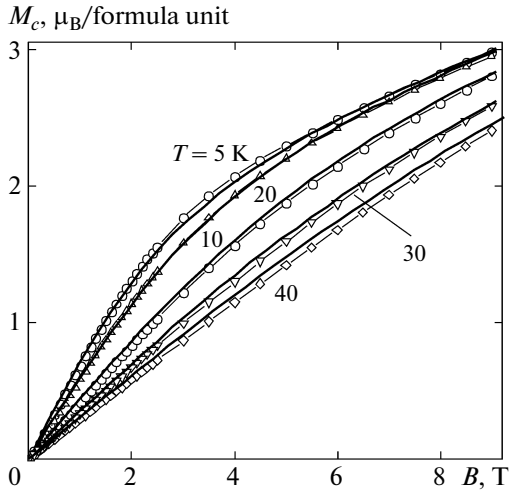

Fig. 3. Magnetization curves of $Sm_{0.7}Ho_{0.3}Fe_3(BO_3)_4$ for **B** ∥ **c** at the given temperatures: (symbols) experimental data and (lines) calculation.

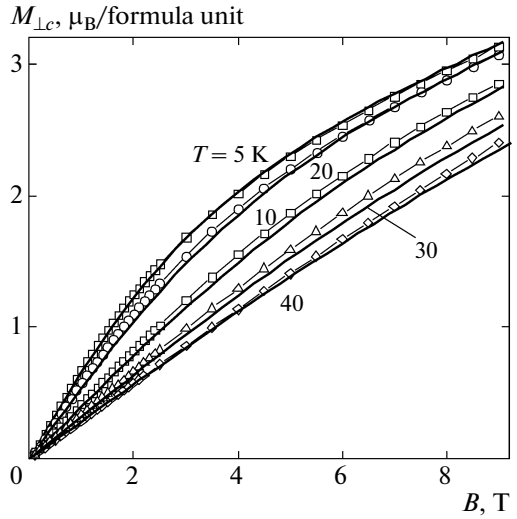

Fig. 4. Magnetization curves of $Sm_{0.7}Ho_{0.3}Fe_3(BO_3)_4$ for **B** ⊥ **c** at the given temperatures: (symbols) experimental data and (lines) calculation.

The $\chi_{c,\perp c}(T)$ curves exhibit a weak anomaly at $T_N \approx 35$ K, which is caused by antiferromagnetic ordering in the Fe subsystem. It is also seen in Fig. 5 that the Néel temperature calculated near T_N is slightly higher than the experimental value, which is the well-known disadvantage of the molecular field approximation. On the whole, the susceptibility curves calculated in the high-temperature range $T_N = 35$–300 K well describe the weakly anisotropic $\chi_{c,\perp c}(T)$ experimental curves.

The calculations demonstrate that the significant increase in the $\chi_{c,\perp c}(T)$ curves at $T < T_N$ detected experimentally is related to the contribution of the holmium part of the R subsystem in $Sm_{0.7}Ho_{0.3}Fe_3(BO_3)_4$. Such an increase in the $\chi_{c,\perp c}(T)$ curves at $T < T_N$ was observed in $HoFe_3(BO_3)_4$ [14, 15], in contrast to $SmFe_3(BO_3)_4$, where $\chi_{\perp c}(T)$ decreases sharply and $\chi_c(T)$ increases weakly with decreasing temperature [3, 11, 30]. On the whole, an increase in $\chi_c(T)$ with decreasing temperature beginning from T_N is characteristic of the easy-plane magnetic anisotropy of the compounds.

The inset to Fig 5 shows the low-temperature regions (for $T < T_N \approx 35$ K) of the experimental and calculated magnetic susceptibility dependences $\chi_{c,\perp c}(T)$. A trigonal crystal with magnetic moments lying in the basal plane can contain three types of antiferromagnetic domains, antiferromagnetism vector **L** in each of which is oriented along the corresponding twofold axis. During magnetization in the basal plane at $B = 0.01$ T, all possible domains contribute to magnetic susceptibility $\chi_{\perp c}(T)$ and the magnetization of $Sm_{0.7}Ho_{0.3}Fe_3(BO_3)_4$ occurs similarly to the processes described in [21] for easy-plane $NdFe_3(BO_3)_4$. Since information on the domain structure of the sample was absent, the domain sizes were assumed to be the same. For a field along axis c, the sample is in the flop phase and behaves like a single-domain sample (Fig. 1a).

The dashed $\chi_{c,\perp c}(T)$ curves shown in the inset to Fig. 5 were calculated on the assumption of a retained easy-plane character of the magnetic subsystem of $Sm_{0.7}Ho_{0.3}Fe_3(BO_3)_4$ at the lowest temperatures. Although the $M_{c,\perp c}(T)$ magnetization curves were successfully described over wide field and temperature

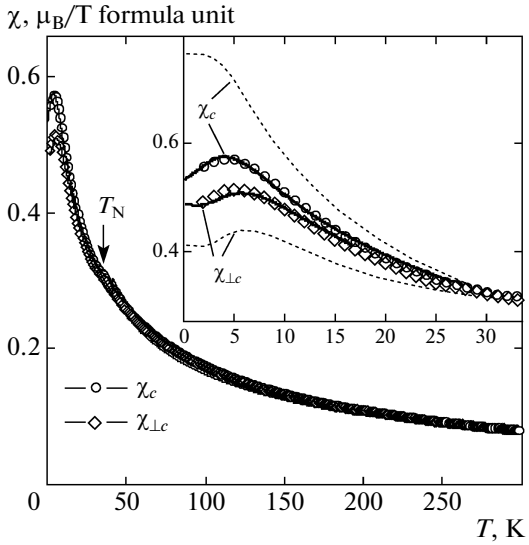

Fig. 5. Temperature dependences of the initial magnetic susceptibility of $Sm_{0.7}Ho_{0.3}Fe_3(BO_3)_4$ for magnetic field directions **B** ∥ **c** and **B** ⊥ **c** at $B = 0.1$ T: (symbols) experimental data and (lines) calculation. (inset) Low-temperature region of the $\chi_{c,\perp c}(T)$ curves at $T < T_N$. (dashed lines) $\chi_{c,\perp c}(T)$ curves calculated on the assumption of an easy-plane anisotropy.

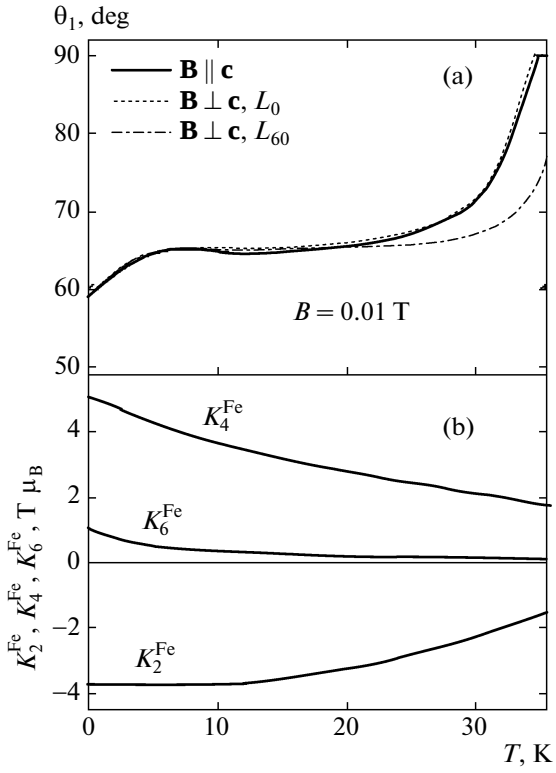

Fig. 6. Temperature dependences of (a) the angle of deviation of the magnetic moment of iron $\mathbf{M}_1^{\mathrm{Fe}}$ from axis c in different domains at $\mathbf{B} \parallel \mathbf{c}$ and $\mathbf{B} \perp \mathbf{c}$ and (b) the anisotropy constants of the iron subsystem $K_{2,4,6}^{\mathrm{Fe}}(T)$.

ranges, the calculated susceptibility $\chi_{c,\perp c}(T)$ curves (dashed lines) are seen to describe the experimental data only qualitatively despite the fact that even the Schottky-type anomaly near $T = 5.5$ K in the $\chi_{\perp c}(T)$ curves is reproduced. The quantitative difference between the calculated and experimental results is most pronounced at the lowest temperatures.

The bad description of the experimental $\chi_{c,\perp c}(T)$ curves is assumed to be related to the misorientation of the sample in the experiment. Indeed, it is clear from an analysis of the $\chi_{c,\perp c}(T)$ curves that, in the case of a misorientation in the experiment and field **B** deviating from axis c through several degrees, the $\chi_{\perp c}(T)$ curve runs slightly lower because of the appearance of a component perpendicular to axis c. Similarly, if a misorientation also take place in measuring $\chi_{\perp c}(T)$, the $\chi_c(T)$ curve runs higher due to the appearance of a component parallel to axis c, which improves the agreement between the calculated and experimental data. However, the calculations performed with allowance for the misorientation showed that the misorientation angle should be at least 15° to improve the agreement between the calculated and experimental results, which is unlikely.

When calculating numerous magnetic phases that could exist in $Sm_{0.7}Ho_{0.3}Fe_3(BO_3)_4$ at various orientations of the magnetic moments of the Sm, Ho, and Fe subsystems, we assumed that the substantial discrepancy between the calculated and experimental data in Fig. 5 can be caused by an off-easy-plane state of the magnetic subsystem at low temperatures. To explain the interesting steplike anomalies in the magnetization and susceptibility curves of $Nd_{1-x}Dy_xFe_3(BO_3)_4$ (x = 0.15, 0.25) in [17], we assumed the presence of a low-temperature magnetic state consisting of a weakly noncollinear antiferromagnetic phase with the magnetic moments of iron deviating from axis c. As a result, using the same set of parameters, we were able to achieve agreement between the calculated and experimental data for the entire set of the measured characteristics of $Nd_{1-x}Dy_xFe_3(BO_3)_4$ [17]. Note that the authors of [31] studied $GdFe_3(BO_3)_4$ exhibiting a spin-reorientation transition and concluded that the magnetic moments of iron deviate from axis c in the easy-axis phase through high angles changing with the temperature and magnetic field (see Fig. 6 in [31]).

The calculations demonstrate that an antiferromagnetic phase with the magnetic moments of Fe deviating from axis c through an angle $\vartheta_1 \approx 63°$ (for $\mathbf{M}_1^{\mathrm{Fe}}$ at $T = 2$ K) and a cone of easy magnetization axes (Fig. 1c) can appear in a trigonal $Sm_{0.7}Ho_{0.3}Fe_3(BO_3)_4$ crystal at low temperatures. This possible state can be caused by the competition of the contributions of the Sm, Ho, and Fe subsystems to the total anisotropy of $Sm_{0.7}Ho_{0.3}Fe_3(BO_3)_4$. The magnetic anisotropy of the iron and samarium subsystems stabilizes an easy-plane magnetic structure (the contribution of the Sm subsystem is very low). At $T_{SR} \approx 4.7$ K, $HoFe_3(BO_3)_4$ undergoes a spin-reorientation transition, which results in an easy-plane magnetic structure at $T < T_{SR}$. In the case of substituted holmium–neodymium ferroborate $Ho_{0.5}Nd_{0.5}Fe_3(BO_3)_4$, the spin-reorientation transition temperature increases noticeably to $T_{SR} \approx$ 9 K. Thus, allowing for a weaker (as compared to the Nd subsystem in $Ho_{0.5}Nd_{0.5}Fe_3(BO_3)_4$) easy-plane contribution of Sm to the magnetic anisotropy of ferroborate $Sm_{0.7}Ho_{0.3}Fe_3(BO_3)_4$, we assume that the contribution of the Ho subsystem to $Sm_{0.7}Ho_{0.3}Fe_3(BO_3)_4$ stabilizes an easy-plane magnetic structure at least to temperatures higher than 9 K.

We now consider the low-temperature specific features of the susceptibility curves of $Ho_{0.5}Nd_{0.5}Fe_3(BO_3)_4$ detected in [15]. It is seen in Fig. 11b from [15] that, as the field increases, temperature T_{SR} in $Ho_{0.5}Nd_{0.5}Fe_3(BO_3)_4$ decreases and the shape of the susceptibility $\chi_c(T)$ curve changes. The $\chi_c(T)$ curve at H = 12 kOe and, especially, 13 kOe tends toward the transition from the easy-plane to the easy-axis state and exhibits a broad peak near T = 3–4 K rather than decreasing sharply at T_{SR} and tending to zero at $T \approx 0$ (which is characteristic of the easy-axis

state). Note hat the broad peak in the $\chi_c(T)$ curve in [15] resembles the anomaly detected in the $\chi_c(T)$ curve of $Sm_{0.7}Ho_{0.3}Fe_3(BO_3)_4$ (see Fig. 5). Thus, the broad peak in the $\chi_c(T)$ curve of $Sm_{0.7}Ho_{0.3}Fe_3(BO_3)_4$ near $T = 5$ K and the subsequent decrease in $\chi_c(T)$ at $T \longrightarrow 0$ can be explained by the tendency toward a change from the easy-plane into the easy-axis state.

The calculations of the $\chi_{c,\perp c}(T)$ curves with the magnetic moments of Fe deviating from axis c demonstrate the possibility of solving the problem related to the substantial discrepancy between the calculated and experimental data on the assumption of an easy-plane state in $Sm_{0.7}Ho_{0.3}Fe_3(BO_3)_4$. It is seen in Fig. 5 and the related inset that the calculated $\chi_{c,\perp c}(T)$ solid curves well describe the experimental data at all temperatures $T < T_N$. The solid $\chi_c(T)$ curve was calculated using the scheme in Fig. 1d, where a weakly noncollinear antiferromagnetic structure forms as a result of the action of field $\mathbf{B} \parallel \mathbf{c}$. When an applied magnetic field lies in the basal plane, the contributions of all three domains to susceptibility $\chi_{\perp c}(T)$ should be taken into account, and the calculation was performed according to the scheme shown in Fig. 1e. The Schottky-type anomaly in the experimental $\chi_{\perp c}(T)$ curve near $T = 5.5$ K is related to the redistribution of the lower level populations for the ground multiplet of the Ho^{3+} ion in $Sm_{0.7}Ho_{0.3}Fe_3(BO_3)_4$, and a correct calculation of the magnetization processes reproduces this effect.

The calculations demonstrate that the R and Fe subsystems in different domains give contributions with different temperature dependences. For example, for $\chi_a(T)$, a domain with an antiferromagnetism axis along an applied field (L_0, $\varphi = 0$) exhibits a nonmonotonic dependence with the Schottky-type anomaly near $T =$ 9.5 K for the rare-earth subsystem. In this case, the Fe subsystem demonstrates a usual parallel antiferromagnet susceptibility increasing with temperature.

The temperature dependences of the contributions of the R and Fe subsystems in domains with antiferromagnetism axes directed at an angle of $\varphi = 60°$ to the field (L_{60}) are slightly different. The Schottky-type anomaly for the rare-earth subsystem is much weaker and the susceptibility decreases with increasing temperature. The susceptibility of the Fe subsystem is nonzero at low temperatures and decreases with increasing temperature. The calculation of $\chi_a(T)$ shows that field $B_a = 0.1$ T tends to rotate L_{60} domains toward the flop state as the temperature increases (see the scheme in Fig. 1e and the text below), and the deviation of vectors $\mathbf{M}_1^{Fe}$ and $\mathbf{M}_2^{Fe}$ from strict collinearity (in plane ab for their inclination to axis a) changes and is 0.10° at $T = 4.2$ K and 0.06° at $T =$ 30 K.

The calculations also demonstrate that the deviation of antiferromagnetic vectors $\mathbf{M}_1^{Fe}$ and $\mathbf{M}_2^{Fe}$ from strict collinearity at $B = 0.01$ T for the calculation of the $\chi_a(T)$ (in domain L_0) and $\chi_c(T)$ dependences increases weakly with the temperature from 0.045° at $T = 2$ K to 0.06° at $T = 30$ K (due to a decrease in the total effective anisotropy constant of the compound).

The calculations indicate that the rotation of the magnetic moments of iron $\mathbf{M}_i^{Fe}$ is different in different domains when the temperature increases and T_N is approached. Figure 6a shows the temperature dependence of the angle of deviation of magnetic moments $\mathbf{M}_1^{Fe}$ from the trigonal axis (ϑ_1) in different domains at $\mathbf{B} \parallel \mathbf{c}$ and $\mathbf{B} \perp \mathbf{c}$. It is seen that the easy magnetization axis direction changes nonmonotonically with the temperature beginning from $\vartheta_1 \approx 59°$ (at $B = 0.01$ T, $T = 0.1$ K for both $\mathbf{B} \parallel \mathbf{c}$ and $\mathbf{B} \perp \mathbf{c}$). For $\mathbf{B} \parallel \mathbf{c}$, the magnetic moments of iron tend to be oriented normal to the field with increasing temperature, and this behavior almost coincides with the character of rotation of the domain with antiferromagnetism axis L_0 at $\mathbf{B} \perp \mathbf{c}$. At $T > 20$ K and $\mathbf{B} \perp \mathbf{c}$, domain L_0 tends to be oriented into the plane faster than two other domains with antiferromagnetism axis L_{60}. Note that the character of a nonmonotonic change in the $\vartheta_1(T)$ dependence for $\mathbf{B} \parallel \mathbf{c}$ at low temperatures mainly determines the resulting shape of the calculated $\chi_c(T)$ curve (in particular, the broad peak near $T = 5$ K). The tendency toward the manifestation of an easy-plane character of the magnetic subsystem of $Sm_{0.7}Ho_{0.3}Fe_3(BO_3)_4$ with increasing temperature (see Fig. 6a) agrees with the results for $HoFe_3(BO_3)_4$ and $Ho_{0.5}Nd_{0.5}Fe_3(BO_3)_4$, where an easy-plane magnetic structure forms with increasing temperature after the spin-reorientation transition.

Figure 6b shows the calculated temperature dependences of the anisotropy constants of the iron subsystem $K_2^{Fe}(T)$, $K_4^{Fe}(T)$, and $K_6^{Fe}(T)$. The magnitude, sign, and character of the $K_{2,4,6}^{Fe}(T)$ dependences demonstrate that the state of a cone of easy magnetization axes (see Fig. 1c) can form at $B = 0$ and that the angle of deviation of the magnetic moments of iron from axis c can change in weak fields $\mathbf{B} \parallel \mathbf{c}$ and $\mathbf{B} \perp \mathbf{c}$ (the character of the $\vartheta_1(T)$ dependence at $B = 0.1$ T is shown in Fig. 6a). The calculations demonstrate that the anisotropy constants of the iron subsystem in the basal plane (K_{33}^{Fe} and $K_{66}^{Fe} \ll K_{2,4}^{Fe}$) should be taken into account at low temperatures in fields $B < 1$ T to compute the $M_{\perp c}(B)$ magnetization curves. The analytical form of the $K_{2,4,6}^{Fe}(T)$ temperature dependences was found from the condition of the best agreement between the experimental and calculated characteristics $\chi_{c,\perp c}(T)$ at $T < T_N$ and $M_{c,\perp c}(B)$ at $B < 1$ T. The found $K_2^{Fe}(T)$ dependence agrees with the Akulov–Zener law

$$\left|K_2^{Fe}\right|(T) \sim \left(\frac{M^{Fe}(T)}{M^{Fe}(0)}\right)^3$$

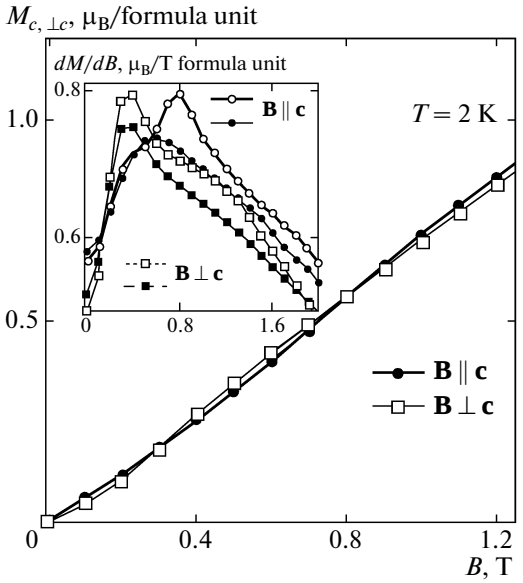

Fig. 7. Low-field region of the experimental magnetization curves of $Sm_{0.7}Ho_{0.3}Fe_3(BO_3)_4$ for **B** || **c** and **B** ⊥ **c** at $T =$ 2 K. (inset) Differential magnetic susceptibility $dM_{c,\perp c}/dB(B)$ at $T =$ (open symbols) 2 and (solid symbols) 5 K.

(see, e.g., [32]). We have $\left|K_2^{Fe}\right| / K_4^{Fe} = 0.85$ at $T = 4.2$ K and $\left|K_2^{Fe}\right| / K_4^{Fe} = 1.13$ at $T = 20$ K. Note that the experimental characteristics of $Sm_{0.7}Ho_{0.3}Fe_3(BO_3)_4$ can be described at lower values of constants $\left|K_2^{Fe}\right|$ and K_4^{Fe} and without regard for K_6^{Fe} using a similar temperature dependence. However, this decrease requires a further decrease in $\left|K_2^{Fe}\right|$; as a result, the $K_4^{Fe} / \left|K_2^{Fe}\right|$ ratio increases sharply and reaches 9–10 at low temperatures.

We now dwell on the low-field region of the experimental $M_{c,\perp c}(B)$ magnetization curves at $T = 2$ K, which is shown separately in Fig. 7 (the curves in Fig. 2 are shown in fields up to 9 T). It is seen that the $M_c(B)$ and $M_{\perp c}(B)$ curves are intersected interestingly (they intersect each other three times with allowance for the high-frequency intersection at $B \approx 5$ T). If the low-temperature $M_{c,\perp c}(B)$ curves are differentiated, the inset to Fig. 7 shows that the curves of differential magnetic susceptibility $dM_{c,\perp c}/dB(B)$ exhibit clear peaks at $B = 0.4$ and 0.8 T (at $T = 2$ K, open symbols) and near $B = 0.36$ and 0.6 T (at $T = 5$ K, solid symbols). A broad peak near $B = 1.2$ T is also visible in the $dM_{c,\perp c}/dB(B)$ curve at $T = 2$ K.

The calculations demonstrate that the detected intersections of the low-temperature $M_{c,\perp c}(B)$ curves at $B < 1.5$ T are caused by the spin-reorientation transitions in the iron subsystem of $Sm_{0.7}Ho_{0.3}Fe_3(BO_3)_4$ from the weakly noncollinear state at an angle to axis c

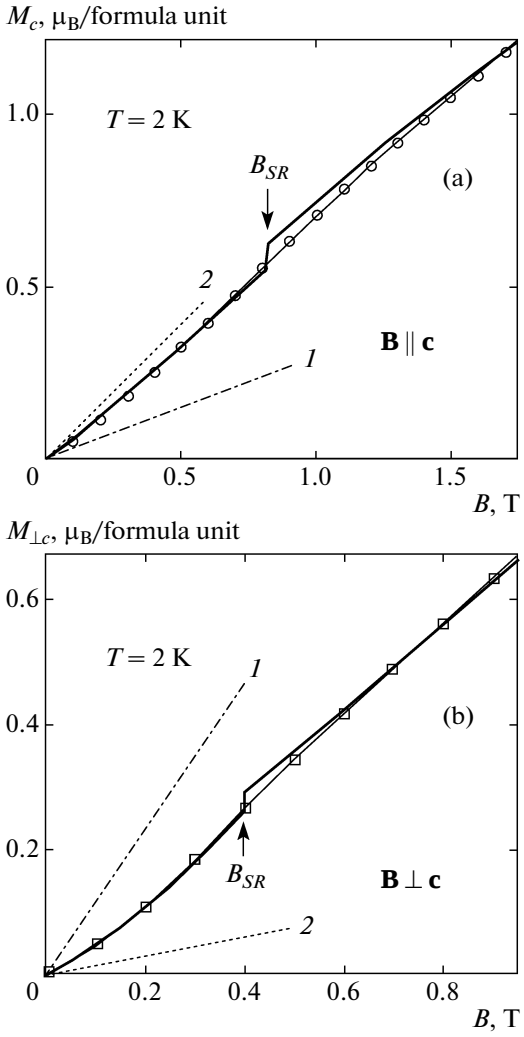

Fig. 8. Low-field region of the experimental magnetization curves of $Sm_{0.7}Ho_{0.3}Fe_3(BO_3)_4$ for **B** || **c** and **B** ⊥ **c** at $T =$ 2 K: (symbols) experimental data and (lines) calculation. (dot-and-dash lines *1*) Easy-axis state and (dashed lines *2*) easy-plane state.

(Figs. 1d, 1e) to the flop state (Figs. 1a, 1b), which take place in close but different critical fields at different directions of an applied magnetic field. At $T = 2$ K, the flop phase for the **B** ⊥ **c** direction forms earlier (at $B_{SR} \approx 0.4$ T) than for the **B** || **c** direction, for which parallel susceptibility stabilizes the initial phase to a higher field ($B_{SR} \approx 0.8$ T).

Calculated dot-and-dash lines *1* for **B** || **c** (Fig. 8a) and **B** ⊥ **c** (Fig. 8b) illustrate the magnetization of $Sm_{0.7}Ho_{0.3}Fe_3(BO_3)_4$ on the assumption of the easy-axis state in low fields beginning from $B = 0$. It is seen that, in the easy-axis state, the magnetization at **B** || **c** is significantly lower and the magnetization at **B** ⊥ **c** is significantly higher than the experimental magnetization. If $Sm_{0.7}Ho_{0.3}Fe_3(BO_3)_4$ is in the easy-axis state at $B = 0$, the calculated magnetization (Fig. 8, dashed lines *2*) corresponds to the calculated $\chi_{c,\perp c}(T)$ suscep-

tibility curves (inset to Fig. 5, dashed lines) and lies above the experimental curve for **B** ∥ **c** (Fig. 8a) and below the experimental curve for **B** ⊥ **c** (Fig. 8b). It is seen from Figs. 8a and 8b that the $M_{c,\perp c}(B)$ solid curves calculated on the assumption of a weakly noncollinear antiferromagnetic phase with the magnetic moments of iron deviating from axis *c* (Figs. 1d, 1e) well describe the experimental data during magnetization in both field **B** ∥ **c** and field **B** ⊥ **c**.

When $Sm_{0.7}Ho_{0.3}Fe_3(BO_3)_4$ is magnetized in the basal plane in fields lower than about 1 T, all three possible domains with antiferromagnetism axes located at an angle of 120° to each other contribute to the magnetization. The $M_{\perp c}(B)$ magnetization curves at $B <$ 1 T were calculated using the approach proposed in [21], where the magnetization processes occurring in easy-plane $NdFe_3(BO_3)_4$ were comprehensively studied with allowance for the possible existence of three types of domains.

During the magnetization in the basal plane for **B** ∥ **a**, the magnetic moments of iron in the domain with antiferromagnetism axis L_0 along an applied field (L_{ab0} is the projection onto the *ab* plane (Figs. 1c, 1e)) make a contribution increasing with the field due to an increase in the inclination to field **B** ∥ **a**. Magnetic moment $\mathbf{m}_{1ab}$ directed opposite to the field in the rare-earth subsystem decreases. As a result, the total magnetization from this domain increases weakly with the field and repeats the experimental $M_{\perp c}(B)$ dependence. In two other domains with antiferromagnetism axes L_{60} located at an angle of $\varphi = 60°$ to the field (which are equivalent with respect to the field direction **B** ∥ **a**), both magnetic moments of iron $\mathbf{M}^{Fe}_{1,2ab}$ in each domain (L_{ab60}) rotate toward the flop state (Fig. 1e). The contribution of the L_{ab60} domain to the magnetization increases due to different rates of $\mathbf{M}^{Fe}_{1,2ab}$ rotation (different lengths of the arrows indicating the direction of $\mathbf{M}^{Fe}_{1,2ab}$ rotation in Fig. 1e corresponds to different rates of rotation). The total magnetization for field **B** ∥ **a**

$$M_a = \frac{1}{2}\left[\frac{1}{3}(M_0^{Fe} + (1-x)m_{1,2a}^{Sm} + xm_{1,2a}^{Ho}) + \frac{2}{3}(M_{60}^{Fe} + (1-x)m_{1,2a}^{Sm} + xm_{1,2a}^{Ho})\right] \quad (11)$$

well describes the experimental $M_{\perp c}(B)$ curve (Fig. 8b). In Eq. (11),

$$M_0^{Fe} = M_1^{Fe}\sin\vartheta_1 - M_2^{Fe}\sin\vartheta_2$$

is the contribution of iron to the magnetization of the L_{ab0} domain with allowance for the projection onto the *ab* plane, and

$$M_{60}^{Fe} = M_1^{Fe}\sin\vartheta_1\cos\varphi_1 + M_2^{Fe}\sin\vartheta_2\cos\varphi_2$$

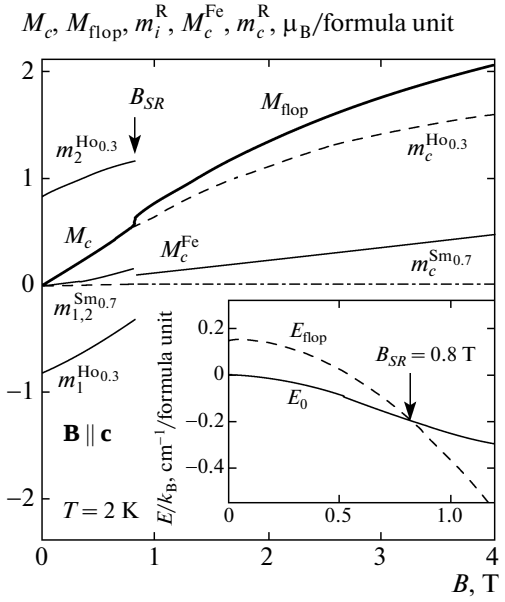

Fig. 9. Calculated field dependences of the components of the *R* and Fe subsystems in $Sm_{0.7}Ho_{0.3}Fe_3(BO_3)_4$ along axis *c* in the initial and flop phases at $T = 2$ K for **B** ∥ **c**. Initial weakly noncollinear phase ($B < B_{SR}$): $\mathbf{m}_1^R$ is the magnetic moment opposite to the field, $\mathbf{m}_2^R$ is the magnetic moment along the field, and M_c is the resulting magnetic moment in the initial phase. Flop phase ($B > B_{SR}$): $\mathbf{m}_c^R$ and M_c^{Fe} are the projections of the rare-earth and iron subsystems along the field, respectively, and M_{flop} is the resulting magnetic moment. (inset) Field dependence of the energies of $Sm_{0.7}Ho_{0.3}Fe_3(BO_3)_4$ in (solid line) initial weakly noncollinear state and (dashed line) flop phase at $T = 2$ K and **B** ∥ **c**.

is the contribution of iron to the magnetization of the L_{ab60} domain with allowance for the projection onto the *ab* plane and the *a* axis.

In a field $B_{SR} \approx 0.4$ T, domain L_0 undergoes a spin-reorientation transition into the flop state, and its magnetization with allowance for the projection onto the *ab* plane is now

$$M_{flop}^{Fe} = M_1^{Fe}\sin\vartheta_1\cos\varphi_1 + M_2^{Fe}\sin\vartheta_2\cos(-\varphi_1)$$

(see Fig. 1b). As a result, the total magnetization for $B > B_{SR}$ is

$$M_a = \frac{1}{2}\left[\frac{1}{3}(M_{flop}^{Fe} + (1-x)m_{1,2a}^{Sm} + xm_{1,2a}^{Ho}) + \frac{2}{3}(M_{60}^{Fe} + (1-x)m_{1,2a}^{Sm} + xm_{1,2a}^{Ho})\right]. \quad (12)$$

When the field increases further, magnetic moments $\mathbf{M}^{Fe}_{1,2ab}$ continue to rotate in domains L_{ab60}, the rate of rotation increases with the field (as shown by the cal-

Table 3. Magnetic moments of the Sm, Ho, and Fe subsystems in the phases in the low-field range at $T = 2$ K ($\mathbf{B} \parallel \mathbf{c}$, $\varphi_1^{\mathrm{Fe}} = 0$, $\varphi_2^{\mathrm{Fe}} = 180°$): $B = 0$ (initial collinear phase at an angle of Fe to axis c), $B = 0.75$ T (weakly noncollinear phase at an angle of Fe to axis c), and $B = 2$ T (flop phase)

m_i^R, M_i^{Fe}	$m_i^R(a, b, c)$, μ_{B}		
	$B = 0$	$B = 0.75$ T	$B = 2$ T
$m_1^{\mathrm{Sm}_{0.7}}$	(−0.2607, 0.01, −0.0066)	(−0.2608, 0.01, −0.0062)	(−0.264, −0.01, 0.001)
$m_2^{\mathrm{Sm}_{0.7}}$	(0.2607, −0.01, 0.0065)	(0.2609, −0.01, 0.0065)	(0.264, −0.01, 0.001)
$m_1^{\mathrm{Ho}_{0.3}}$	(−1.72, 0.25, −0.83)	(−1.73, 0.12, −0.37)	(−1.75, −0.35, 1.11)
$m_2^{\mathrm{Ho}_{0.3}}$	(1.72, −0.25, 0.83)	(1.71, −0.33, 1.14)	(1.75, −0.35, 1.11)
M_1^{Fe}	ϑ_1, $M_{1c}^{\mathrm{Fe}} = M_1^{\mathrm{Fe}}\cos\vartheta_1$ ($M_1^{\mathrm{Fe}} = 15\mu_{\mathrm{B}}$, $\varphi_1^{\mathrm{Fe}} = 0$)		
	62.857°, 6.843μ_{B}	63.031°, 6.803μ_{B}	89.125°, 0.229μ_{B}
M_2^{Fe}	ϑ_2, $M_{2c}^{\mathrm{Fe}} = M_2^{\mathrm{Fe}}\cos\vartheta_2$ ($M_2^{\mathrm{Fe}} = 15\mu_{\mathrm{B}}$, $\varphi_2^{\mathrm{Fe}} = 180°$)		
	117.143°, −6.843μ_{B} ($180° - \vartheta_2 - \vartheta_1 = 0$)	115.881°, −6.553μ_{B} ($180° - \vartheta_2 - \vartheta_1 = 1.088°$)	89.125°, 0.229μ_{B}

culations), and the resulting magnetization becomes close to the flop-phase magnetization beginning from a field of about 1 T. The inflection point in the $dM_{\perp c}/dB(B)$ curve near $B = 1.2$ T at $T = 2$ K (Fig. 7, inset) is likely to be related to the transition of L_{60} domains into the flop state. Note that the rotations and jumps of the magnetic moments of iron in domains are accompanied by changes in the components of the magnetic moments of the rare-earth subsystem. These components were calculated using the generally accepted formalism described in Section 3, which takes into account that an R ion undergoes the action of the crystal field and is magnetized by the exchange field of iron and applied magnetic field **B**.

The weak magnetization jump in the $M_c(B)$ curves at a field $B_{SR} \approx 0.8$ T in Fig. 8a is caused by the spin-reorientation transition in the iron subsystem from the initial weakly noncollinear phase (Fig. 1d) into the flop phase (Fig. 1a) and is accompanied by the reorientation of the magnetic moments of the Sm^{3+} and Ho^{3+} ion sublattices along field $\mathbf{B} \parallel \mathbf{c}$. Figure 9 shows the field dependences of the components of the magnetic moments of the R and Fe subsystems in $Sm_{0.7}Ho_{0.3}Fe_3(BO_3)_4$ along axis c at $T = 2$ K for $\mathbf{B} \parallel \mathbf{c}$. These dependences are presented for $\mathbf{m}_{1c}^{\mathrm{R}}$ (magnetic moment opposite to the field direction) and $\mathbf{m}_{2c}^{\mathrm{R}}$ (along the field), and the resulting magnetization is shown for the initial phase,

$$M_c = \frac{1}{2}(M_1^{\mathrm{Fe}}\cos\vartheta_1 + M_2^{\mathrm{Fe}}\cos\vartheta_2 + (1-x)m_{1,2c}^{\mathrm{Sm}} + xm_{1,2c}^{\mathrm{Ho}})$$

and the flop phase,

$$M_{\mathrm{flop}} = \frac{1}{2}(M_{1,2c}^{\mathrm{Fe}} + (1-x)m_{1,2c}^{\mathrm{Sm}} + xm_{1,2c}^{\mathrm{Ho}}).$$

The small difference between the values of M_c and M_{flop} in a field $B_{SR} \approx 0.8$ T is mainly caused by a change in the contributions of the Ho and Fe subsystems. Table 3 gives the magnetic moments of the Sm, Ho, and Fe subsystems in the phases under study in the low-field range at $T = 2$ K, $\mathbf{B} \parallel \mathbf{c}$, $\varphi_1^{\mathrm{Fe}} = 0$, and $\varphi_2^{\mathrm{Fe}} = 180°$. The second column contains the magnetic moments at $B = 0$ in the initial collinear antiferromagnetic phase at an angle to axis c (Fig. 1c). The third column gives the magnetic moments in the weakly noncollinear antiferromagnetic phase at an angle to axis c for $B = 0.75$ T (Fig. 1d). The last column presents the magnetic moments in the flop phase at $B = 2$ T (Fig. 1a).

The inset to Fig. 9 shows the field dependence of the energies of $Sm_{0.7}Ho_{0.3}Fe_3(BO_3)_4$ at $T = 2$ K in the initial weakly noncollinear state (E_0), in which the magnetic moments of Fe deviate from axis c (solid

line), and in the flop phase (E_{flop}, dashed line). It is seen that, in fields up to 0.8 T, the state with E_0 is the most favorable state of the magnetic subsystem in $Sm_{0.7}Ho_{0.3}Fe_3(BO_3)_4$ (Fig. 1d, solid line); then, as the field increases, the flop phase forms beginning from $B_{SR} = 0.8$ T (Fig. 1a, dashed line).

Thus, when calculating the magnetization of $Sm_{0.7}Ho_{0.3}Fe_3(BO_3)_4$ in the basal plane and along the trigonal axis, we were able to describe the experimental magnetization curves in fields up to 1 T, which indicate phase transitions. Note that we used one set of parameters (see Table 2) and anisotropy constants $K^{Fe}_{2,4,6,33,66}$ and used no adjustable parameters to calculate the $\chi_{c,\perp c}(T)$ susceptibility curves in the ordered and paramagnetic temperature ranges and to calculate the field dependences of the $M_{c,\perp c}(B)$ magnetization curves up to 9 T.

CONCLUSIONS

We experimentally and theoretically studied the magnetic properties of substituted ferroborate $Sm_{0.7}Ho_{0.3}Fe_3(BO_3)_4$ with competing Sm–Fe and Ho–Fe exchange interactions and achieved good agreement between the calculated and experimental data for the entire set of the measured characteristics. Using a general theoretical approach based on the crystal field model for a rare-earth ion and the molecular field approximation, we were able to determine the actual parameters of $Sm_{0.7}Ho_{0.3}Fe_3(BO_3)_4$ by comparing the calculated and experimental results.

Weakly anisotropic behavior of the magnetic characteristics of $Sm_{0.7}Ho_{0.3}Fe_3(BO_3)_4$, which is unique for ferroborates, was detected over almost the entire temperature range under study and was then explained. Assuming an easy-pane character of the magnetic subsystem of $Sm_{0.7}Ho_{0.3}Fe_3(BO_3)_4$, we correctly described the experimental $M_{c,\perp c}(B)$ curves for $B > 1.2$ T. The substantial discrepancy between the calculated and experimental $\chi_{c,\perp c}(T)$ curves at low temperatures was removed on the assumption of the appearance of an antiferromagnetic state with the magnetic moments of iron deviating from axis c (at $T = 2$ K, the angle of deviation is 63°) beginning from $B = 0$. The proposed version of the magnetization processes occurring in low magnetic fields allowed us to comprehensively analyze the behavior of the magnetic moments of the R and Fe subsystems and to describe the nonlinear low-temperature $M_{c,\perp c}(B)$ curves, which indicate phase transitions from the initial phase into a flop phase.

We achieved good agreement between the experimental and calculated temperature dependences $\chi_{c,\perp c}(T)$ in the paramagnetic temperature range at $\Theta = -170$ K. The detected anomalies in the $\chi_{c,\perp c}(T)$ curves below the Néel temperature were shown to be described using the competing contributions of the Sm, Ho, and Fe subsystems to the total anisotropy of $Sm_{0.7}Ho_{0.3}Fe_3(BO_3)_4$ with allowance for possible existence of three types of domains in a crystal of trigonal symmetry.

ACKNOWLEDGMENTS

The authors thank D.I. Sirota for fruitful discussions and his interest in this research.

REFERENCES

1. A. K. Zvezdin, S. S. Krotov, A. M. Kadomtseva, G. P. Vorob'ev, Yu. F. Popov, A. P. Pyatakov, L. N. Bezmaternykh, and E. A. Popova, JETP Lett. **81** (6), 272 (2005).
2. A. K. Zvezdin, G. P. Vorob'ev, A. M. Kadomtseva, Yu. F. Popov, A. P. Pyatakov, L. N. Bezmaternykh, A. V. Kuvardin, and E. A. Popova, JETP Lett. **83** (11), 509 (2006).
3. A. M. Kadomtseva, Yu. F. Popov, G. P. Vorob'ev, A. P. Pyatakov, S. S. Krotov, K. I. Kamilov, V. Yu. Ivanov, A. A. Mukhin, A. K. Zvezdin, A. M. Kuz'menko, L. N. Bezmaternykh, I. A. Gudim, and V. L. Temerov, Low Temp. Phys. **36** (6), 511 (2010).
4. Yu. F. Popov, A. M. Kadomtseva, G. P. Vorob'ev, A. A. Mukhin, V. Yu. Ivanov, A. M. Kuz'menko, A. S. Prokhorov, L. N. Bezmaternykh, and V. L. Temerov, JETP Lett. **89** (7), 345 (2009).
5. I. A. Gudim, E. V. Eremin, and V. L. Temerov, J. Cryst. Growth **312**, 2427 (2010).
6. A. K. Zvezdin, A. M. Kadomtseva, Yu. F. Popov, G. P. Vorob'ev, A. P. Pyatakov, V. Yu. Ivanov, A. M. Kuz'menko, A. A. Mukhin, L. N. Bezmaternykh, and I. A. Gudim, JETP **109** (1), 68 (2009).
7. R. P. Chaudhury, F. Yen, B. Lorenz, Y. Y. Sun, L. N. Bezmaternykh, V. L. Temerov, and C. W. Chu, Phys. Rev. B: Condens. Matter **80**, 104424 (2009).
8. G. A. Zvyagina, K. R. Zhekov, I. V. Bilych, À. À. Zvyagin, L. N. Bezmaternykh, and I. À. Gudim, Low Temp. Phys. **36** (3), 279 (2010).
9. A. V. Malakhovskii, E. V. Eremin, and D. A. Velikanov, A. V. Kartashev, A. D. Vasil'ev, and I. A. Gudim, Phys. Solid State **53** (10), 2032 (2011).
10. E. P. Chukalina, M. N. Popova, L. N. Bezmaternykh, and I. A. Gudim, Phys. Lett. A **374**, 1790 (2010).
11. Yu. F. Popov, A. P. Pyatakov, A. M. Kadomtseva, A. K. Zvezdin, A. A. Mukhin, V. Yu. Ivanov, and I. A. Gudim, JETP **111** (2), 199 (2010).
12. A. A. Mukhin, G. P. Vorob'ev, V. Yu. Ivanov, A. M. Kadomtseva, A. S. Narizhnaya, A. M. Kuz'menko, Yu. F. Popov, L. N. Bezmaternykh, and I. A. Gudim, JETP Lett. **93** (5), 275 (2011).
13. A. M. Kuz'menko, A. A. Mukhin, V. Yu. Ivanov, A. M. Kadomtseva, and L. N. Bezmaternykh, JETP Lett. **94** (4), 294 (2011).
14. C. Ritter, A. Vorotynov, A. Pankrats, G. Petrakovskii, V. Temerov, I. Gudim, and R. Szymczak, J. Phys.: Condens. Matter **20**, 365209 (2008).
15. R. P. Chaudhury, F. Yen, B. Lorenz, Y. Y. Sun, L. N. Bezmaternykh, V. L. Temerov, and C. W. Chu, Phys. Rev. B: Condens. Matter **80**, 104424 (2009).

16. A. Pankrats, G. Petrakovskii, A. Kartashev, E. Eremin, and V. Temerov, J. Phys.: Condens. Matter **21**, 436001 (2009).
17. A. A. Demidov, I. A. Gudim, and E. V. Eremin, JETP **114** (2), 259 (2012).
18. A. A. Demidov, I. A. Gudim, and E. V. Eremin, Physica B (Amsterdam) **407**, 393 (2012).
19. A. A. Demidov and D. V. Volkov, Phys. Solid State **53** (5), 985 (2011).
20. E. A. Popova, D. V. Volkov, A. N. Vasiliev, A. A. Demidov, N. P. Kolmakova, I. A. Gudim, L. N. Bezmaternykh, N. Tristan, Yu. Skourski, B. Büuchner, C. Hess, and R. Klingeler, Phys. Rev. B: Condens. Matter **75**, 224413 (2007).
21. D. V. Volkov, A. A. Demidov, and N. P. Kolmakova, JETP **104** (6), 897 (2007).
22. D. V. Volkov, A. A. Demidov, and N. P. Kolmakova, JETP **106** (4), 723 (2008).
23. A. A. Demidov, N. P. Kolmakova, D. V. Volkov, and A. N. Vasiliev, Physica B (Amsterdam) **404**, 213 (2009).
24. A. A. Demidov and D. V. Volkov, Phys. Solid State **54** (3), 537 (2012).
25. Y. Hinatsu, Y. Doi, K. Ito, M. Wakeshima, and A. Alemi, J. Solid State Chem. **172**, 438 (2003).
26. S. A. Klimin, D. Fausti, A. Meetsma, L. N. Bezmaternykh, P. H. M. Van Loosdrecht, and T. T. M. Palstra, Acta Crystallogr., Sect. B: Struct. Sci. **61**, 481 (2005).
27. B. J. Wybourne, *Spectroscopic Properties of Rare Earths* (Wiley, New York, 1965), p. 171.
28. A. K. Zvezdin, V. M. Matveev, A. A. Mukhin, and A. I. Popov, *Rare Earth Ions in Magnetically Ordered Crystals* (Nauka, Moscow, 1985) [in Russian].
29. I. E. Dzyaloshinskii, Sov. Phys. JETP **5** (6), 1259 (1957).
30. A. A. Demidov, D. V. Volkov, I. A. Gudim, and E. V. Eremin, *Proceedings of 36th Conference on the Low Temperature Physics LT-36, St.-Petersburg, 2012*, p. 153.
31. S. A. Kharlamova, S. G. Ovchinnikov, A. D. Balaev, M. F. Thomas, I. S. Lyubutin, and A. G. Gavriliuk, JETP **101** (6), 1098 (2005).
32. S. V. Vonsovskii, *Magnetism* (Nauka, Moscow, 1971; Wiley, New York, 1974).

Translated by K. Shakhlevich